www.czasopisma.pan.pl PAN POLSKA AKADEMIA NAUK www.journals.pan.pl

Arch. Metall. Mater. **67** (2022), 3, 967-974

DOI: https://doi.org/10.24425/amm.2022.139690

NANFU ZONG[1,2*], SIDA MA[2], WEIZHAO SUN[2], YANG LIU[3], TAO JING[2]

NUMERICAL MODELLING OF CHAMFER BILLET OF HIGH CARBON STEEL DURING CONTINUOUS CASTING

The formation of internal cracks in as-cast billet is mainly attributed to the stress and strain states near the solidifying front. This study investigates the effect of chamfer configuration of as-cast billet on the maximal principal stress and the tensile stress during soft reduction process. The LIT and ZDT of GCr15 bearing steel are calculated by the solidification phase transformation model. What's more, the 3D finite element models is established to investigate stress and strain states in the brittle temperature range. The relationships between chamfer angle and maximal principal stress, internal crack, as well as equivalent plastic strain are analyzed. Numerical results reveal that a chamfer configuration of as-cast billet is much more effective than a rectangular one on decreasing the risk of internal cracks.

Keywords: chamfer billet; internal cracks; GCr15 steel; soft reduction

1. Introduction

As one of the most commonly used high-chromium bearing steels, GCr15 steel (AISI-52100) has the characteristics of high wear resistance, corrosion resistance and good dimensional stability. It has been widely used in manufacturing bearing ring, ball screw and other mechanical components. GCr15 steel is a high carbon and high chromium bearing steel, which easily leads to a major quality problem of center segregation and internal porosity during continuous casting process [1]. In order to improve the product quality and to develop high profit products, an effective way should be adopted to minimize the internal defects of GCr15 as-cast billet.

The soft reduction technology was originated by mechanical reduction on the as-cast billet to compensate the solidification shrinkage, which successfully alleviates the center segregation and porosity in billet [2,3]. However, internal cracks are always observed in high carbon as-cast billets. Understanding the mechanical behavior of the mushy zone during continuous casting process is important to obtain good quality products, because of internal cracks observed in as-cast steels are almost originated in the mushy zone. The internal cracks is mainly attributed to the strength and ductility in the mushy zone between the liquid impenetrable temperature (LIT) and the zero ductility temperature (ZDT) [4]. When the applied tensile stress exceeds the critical fracture stress or the accumulated strain exceeds the critical strain, cracks will be initiated in the as-cast billet.

Numerical simulations method has been widely used to analyze and optimize the casting process [5-9]. Many researchers [10,11] have investigated the stress and strain in as-cast billets, to estimate the cracking tendency under the soft reduction process. However, previous studies did not provide any investigation how surface profiles of as-cast billet to influence on internal cracks under soft reduction. Chamfering corners is a common idea when facing corner cracks problems [12,13]. Here, this idea is applied to decrease risk of internal cracks after soft reduction. The present study is examined how billet surface profiles lighten internal cracks and analyzed the crack susceptibility by simulating the soft reduction process with finite element method. This is significantly different from the regular continuous casting process, and few publications have studied the evolution of chamfer billet under the soft reduction. In addition, chamfer billet of steel is also appropriate for endless/direct casting and rolling technologies with zero emissions for billet reheating through gas furnaces, and endless/direct casting and rolling technologies coupling with chamfer mold technology

[1] R&D INSTITUTE OF BENGANG STEEL PLATES CO., LTD., BENXI 117000, CHINA
[2] TSINGHUA UNIVERSITY, KEY LABORATORY FOR ADVANCED MATERIALS PROCESSING TECHNOLOGY, MINISTRY OF EDUCATION, SCHOOL OF MATERIALS SCIENCE AND ENGINEERING, BEIJING 100084, CHINA
[3] JIANGSU CHANGQIANG IRON AND STEEL CORP., LTD., JIANGSU 214500, CHINA

* Corresponding author: zongnan512712_2005@163.com

can fulfill the demands for high efficiency and energy savings in production of spooled coils and wire rod.

In the present work, the influence of differential chamfer profile on evolution of internal crack in as-cast billet during the soft reduction was investigated with numerical simulation method for the first time, which aims to provide theoretical basis for designing soft reduction and thus effectively improving the internal crack. In this paper, optimal design of a chamfer profile (chamfer angle and chamfer length) to as-cast billet has been proposed and a 3D finite element model using commercial finite element software ABAQUS® was developed to obtain stress and strain distribution.

2. Theory section

2.1. Solidification Phase Transformation Model of GCr15 in Mushy Zone

In order to obtain the liquid impenetrable temperature (LIT) and the zero ductility temperature (ZDT), the characteristics of solute enrichment in the mushy zone of a billet was investigated for the casting of bearing steel GCr15. It is interesting to note that the degree of solute enrichment of each element (C, Si, Mn, P, S and Cr) in the mushy zone decreases initially and then increases with the increase in centre solid fraction. Consequently, the mushy zone could be divided into the mass/liquid feeding zone ($0.4 < fs < 0.9$) and the cracking zone ($0.9 < fs < 0.99$) [14]. The cracks have a relation with the strength and ductility in the mushy zone between the liquid impenetrable temperature (LIT) and the zero ductility temperature (ZDT), which can be seen in Fig. 1. The steel has no strength and no ductility, and behaves as the liquid above the zero strength temperature (ZST). Hot tears can be refilled with surrounding liquid and left no cracks in ZST and LIT range. Cracks formed in the mass/liquid, whereas cracks formed in the cracking zone and cannot be refilled with liquid, because the dendrite arms are close enough to resist the surrounding liquid feeding. Therefore, the temperature between LIT and ZDT is known as the brittle temperature range. In the continuously cast billet, the microsegregation has been calculated using the direct difference method suggested by Ueshima [15].

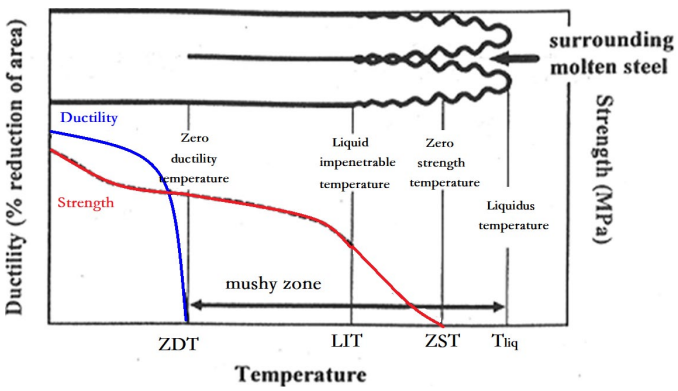

Fig. 1. Schematic diagram of mechanical properties near melting point during continuous casting of steels

The morphology of the growing dendrite array is schematically shown in Fig. 2(a), and the transverse cross-section of dendrites is assumed to be a regular hexagon approximately, one-sixth of which is divided into 100 parts for calculation of interdendritic solute diffusion as schematically shown in Fig. 2(b). The following one-dimensional solute diffusion equation is solved in the triangular domain. In the axial direction of dendrite, the diffusion in solid and liquid is assumed to be negligible. Between δ-Fe and liquid phase, γ-Fe could be developed from the interface. The solute concentrations are assumed to be in the local equilibrium in the solid-liquid and δ/γ interfaces. The equilibrium distribution coefficient between γ-Fe and δ-Fe is assumed to beDuring the δ/γ transformation, sulfur, silicon and phosphorus, for which $K^{\gamma/\delta} < 1$, are redistributed from γ-Fe to δ-Fe, but carbon and manganese, for which $K^{\gamma/\delta} > 1$, are redistributed from δ-Fe to γ-Fe. Diffusion of dendrite will be calculated in X direction of the triangular MOP in Fig. 2(b) by one-dimensional diffusion. When the liquid temperature (T_{Liq}) and the δ/γ transformation temperature (T_{Ar4}) become equal to the actual temperature of the sample, the δ/γ transformation and solidification in one part are completed and the interface moves to the next part. T_{Liq} and T_{Ar4} are shown as the following Eq. (1) and Eq. (2).

$$T_{Liq} = T_P - \sum_i m_i \cdot C_{l,i}^0 \tag{1}$$

$$T_{Ar4} = T_p^{\delta/\gamma} - \sum_i n_i \cdot k_i^{\delta/l} C_{l,i}^{\delta} \tag{2}$$

Where T_p is the melting point of pure iron (1536), and $T_p^{\delta/\gamma}$ is the temperature of the δ/γ transformation of pure iron (1392°C), $C_{l,i}^0$ and $C_{l,i}^{\delta}$ are the concentration of each solute element i in initial liquid phase and at the liquid/δ interface respectively,

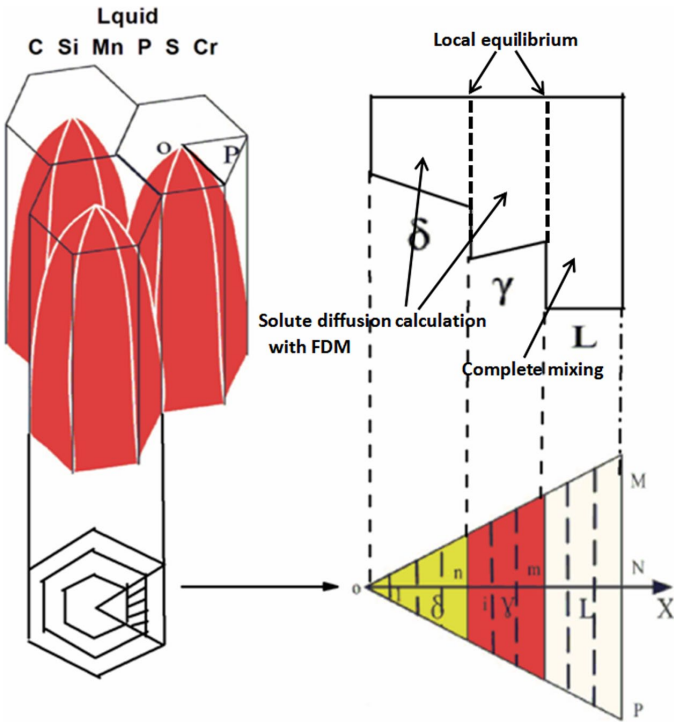

Fig. 2. (a) Schematic drawing showing the morphology of the dendrite array and (b) the transverse cross section assumed in calculated model

m_i and n_i are the slope of liqudus line and δ/γ transformation line of each solute element i in its pseudo-binary Fe-i diagram respectively.

Due to the above assumption, solute diffuses completely in the liquid phase, and diffuses limited in the solid phase. The solute concentration will be obtained by Fick's second law as the following Eq. (3).

$$\frac{\partial C_{S,i}}{\partial} = \frac{\partial}{\partial x}\left[D_{S,i}(T)\frac{\partial C_{S,i}}{\partial x} \right] \tag{3}$$

Where $C_{S,i}$ is the concentration of each solute element i in solid phase, $D_{S,i}(T)$ is the diffusion coefficient of each solute element i in the solid phase when the temperature is T.

The initial conduction is described as the Eq. (4), and the Eq. (5) is the boundary conditions of the model. Where C_0 is the initial solute concentration in the liquid phase, is the space between primary crystallization.

$$C_S = k^{S/L} \cdot C_0, \text{ at } t = 0 \tag{4}$$

$$(\partial C_S)/\partial x = 0, \text{ at } x = 0,\ \lambda_{PDAD}/2 \tag{5}$$

The chemical composition of the steel GCr15 is shown in TABLE 1. The brittle temperature range is between LIT ($f_s = 0.9$) and ZDT ($f_s = 0.99$) [16]. The LIT and ZDT will be calculated by the solidification phase transformation model.

TABLE 1

Chemical composition of steel GCr15 (in mass %)

C	Si	Mn	Cr	P	S
0.96	0.19	0.36	1.46	0.013	0.006

2.2. Billet Mechanical Reduction Model

For the calculations of temperature, stress and strain in the billets during soft reduction, fully coupled thermo-mechanical finite element models have been developed using the software ABAQUS. The first step of this model is to understand the temperature distribution in the billets when it is rolled by the soft reduction rolls, however, temperature calculation model is introduced in detail elsewhere [11,12]. Then the temperature fields were transferred to the rolling model as the initial temperature fields. The soft reduction model is created with ABAQUS/Explicit to calculate the stress and strain fields in the billets with soft reduction. In the soft reduction model, rolls and billets are assumed to be discrete rigid and deformable body, respectively. Since the yield stress of the billets is much lower than that of the rolls. One quarter of the billet is modeled, due to the symmetry of the deformation behavior of the billets in the soft reduction process. Fig. 3 shows the geometry and mesh of the model. The thickness reduction assigned to each billet was 2 mm and the casting speed was set to 0.46 m·min^{-1}.

Reduced integration has been used for improved accuracy of finite element approximations, the family of element library

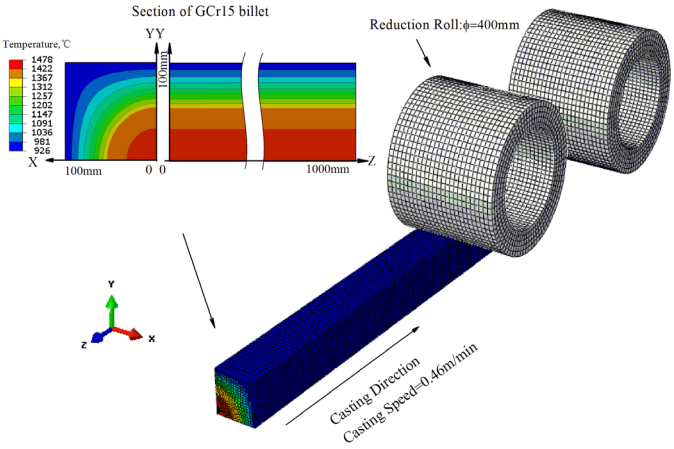

Fig. 3. Geometry and mesh of the finite element model

is coupled temperature-displacement. Element shape is hex and technique is structured. Element size was gradually coarsened from the surfaces of the bloom into the bloom interior region. In addition, 43500 elements have been generated on part of as-cast billet. In this model, the thermo-physical properties of the billet which change with temperature such as density, Young's modulus, thermal conductivity, specific heat capacity, thermal expansion coefficient, change with temperature and are taken from Refs [17-18]. The billets use nonlinear isotropic hardening material model. Material behavior is considered to formulate the constitutive equation of the GCr15 steel, the constitutive equation considering the compensation of strain rate during hot deformation could predict the flow stress throughout the entire temperature and strain rate ranges precisely [19,20]. The results show that the flow stress values predicted by the developed constitutive equation are agree well with the experimental values, which confirm the accuracy and reliability of the proposed deformation constitutive equation of GCr15 steel.

The constitutive equation of GCr15 has been taken at low temperature [17], which can be formulated as following Eq. (6):

$$\sigma\big|_{950<T<1150} = \frac{1}{\alpha}\ln\left\{\left(\frac{\acute{\varepsilon}^{4/3}\exp\left(\frac{Q}{RT}\right)}{A}\right)^{1/n} + \left[\left(\frac{\acute{\varepsilon}^{4/3}\exp\left(\frac{Q}{RT}\right)}{A}\right)^{2/n} + 1\right]^{1/2}\right\} \tag{6}$$

Where σ is the true stress (MPa); n is the materials stress index; $\acute{\varepsilon}$ is the strain rate (s^{-1}); Q is the activation energy of hot deformation (kJ mol^{-1}); T is the absolute temperature (K); R is the universal gas constant (8.31 J mol^{-1}K^{-1}); A and α are the materials constants. When the temperature of billets is from 950°C to 1150°C, the flow stress was determined by the above model. The flow stress obtained from a simple constitutive equation is consistent with the above equation at this temperature region

[21]. The simple constitutive equation is judged on its ability to reproduce experimental data from both tensile and creep tests and its ability to exhibit reasonable behavior under complex loading conditions. The equations are suitable for small strain monotonic loading conditions for a wide range of low strain rates (10^{-3} to 10^{-6} s^{-1}), high temperatures (950°C to 1400°C) and varying carbon contents (0.005 to 1.54 wt. %). Therefore, when the temperature of billets is from 1150°C to *ZST*, the material model proposed by Lee and Kim was used to obtain the flow stress in the mushy zone. The simple constitutive equation of GCr15 at high temperature has been taken at low temperature [21], which can be formulated as following Eq. (7):

$$\sigma = \left(\frac{\dot{\varepsilon}}{C \exp\left(\frac{-Q}{T} \right)} \right)^{1/n} + a_\varepsilon \varepsilon_P^{n_\varepsilon} \tag{7}$$

Where

$$C = 46550 + 71400\,[\mathrm{C\%}] + 12000\,[\mathrm{C\%}]^2$$

$$Q = 44650$$

$$a_\varepsilon = 130.5 - 5.128 \times 10^{-3} T$$

$$n_\varepsilon = -0.6289 + 1.114 \times 10^{-3} T$$

$$n = 8.132 - 1.540 \times 10^{-3} T$$

Where σ is the true stress (MPa); n is the materials stress index; $\dot{\varepsilon}$ is the strain rate (s^{-1}); ε_p is the inelastic strain (m/m); Q is the activation energy of hot deformation (kJ mol^{-1}); T is the absolute temperature (K); [C%] is the carbon content of slab (wt. %).

When the temperatures exceeding *ZST*, steel has neither strength nor ductility and behaves as a liquid above *ZST* [22]. The flow stress of liquid steel was determined and regarded as a pure hydrostatic pressure equal to the current ferrostatic pressure when the temperature is higher than the *ZST* as following Eq. (8).

$$\sigma_{T=T_{liquid}} = P_{hydrostatic\ pressure} \tag{8}$$

Where $\sigma_{T=T_{liquid}}$ is the true stress when the temperatures is higher than the *ZST* (MPa); $P_{hydrostatic\ pressure}$ is the ferrostatic pressure acts on the interface between liquid and solidifying shell when the temperatures exceeding *ZST* (MPa).

When the temperature of billet is above *ZST* and exceeding liquidus of steel, the flow stress can be obtained from the following Eq. (9).

$$\sigma\Big|_{T_{ZST}<T<T_{Liquidus}} = \frac{(T - T_{ZST})\sigma\Big|_{T=T_{Liquidus}} + (T_{Liquidus} - T)\sigma\Big|_{T=T_{ZST}}}{T_{Liquidus} - T_{ZST}} \tag{9}$$

During the soft reduction process, the temperature of billets is cooled down by the cold rolls through heat conduction. Then a severe decrease in temperature is found at the surface of the billets.

3. Results and discussion

Five different mold corner configurations have been considered in the Fig. 4, the length of h is 25 mm, and the angles (α) of chamfer are 0°, 30°, 45°and 60°. There are two pairs pinch of reduction rolls considered in the soft reduction model, and the amount of reduction in each pair pinch rolls is 2 mm. When the equivalent plastic strain and the larger tensile stress is larger than the critical fracture strain and critical stress, respectively, the internal cracks are more easily to form in the brittle temperature range.

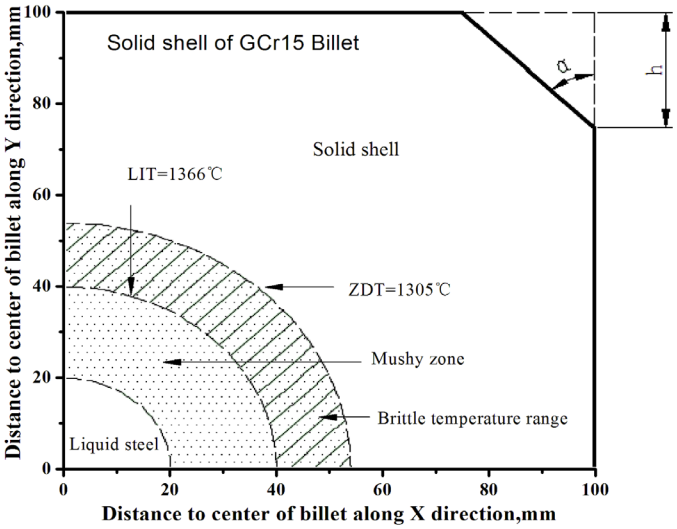

Fig. 4. Section of chamfer GCr15 billet during soft reduction

They are calculated that LIT is 1366°C and *ZDT* is 1305°C by the solidification phase transformation model. Internal cracks will possibly be generated, when the equivalent plastic strain is larger than the critical strain. Strength and ductility are lower in the mushy zone between *ZDT* and LIT those in the other zones because of the existence of interdendritic liquid films at grain boundaries. Therefore, the tensile deformation in this temperature range can cause internal cracks to form when strain and stress reach their critical values. All the cracks that form in the solidification front during soft reduction are sensitive not only to strain but also to stress. In general, the possibility of internal cracks can be estimated by a comparison of the equivalent plastic strain and stress with the critical values in the mushy zone.

A. Yamanaka et al. [23] have found the critical strain value lies between 0.5% and 1.5% for steels with a carbon content of 1.0 wt. % and the deformation strain rate of 10^{-2}-10^{-4} s^{-1}. In order to reveal the effect of steel composition more clearly, Hiebler et al. [24] have showed the relation between the critical strain, carbon equivalent (Cp), and the ration of Mn/S from three pertinent studies by the laboratory bending-type test, where Cp = C+0.02Mn+0.004Ni-0.1Si-0.04Cr-0.1Mo. Thus, in this article, the critical strain value for evaluating the internal cracks is assumed to be 0.4 %.

The high reduction intensities should be avoided especially at the beginning of the reduction process, the soft reduction

amount of the first and second roll is reduced 2 mm. It can be seen from Fig. 5 and Fig. 6 that the equivalent plastic strains in the brittle temperature range of different billet with different chamfer are illustrated during soft reduction. The field of strain under first pinch roll is lower than that under second pinch roll, which is always positive and the equivalent plastic strain decreases with the increasing of α. The maximum of strain decreases from about 0.352% at the angle of 0°, and it subsequently decreases to about 0.082% near the angle of 30°, and it increases to about 0.097% with increasing the angle. The equivalent plastic strain with a soft reduction of 2 mm under first pinch roll is less than the critical stress, however, when the angle of billet is 0, the equivalent plastic strain is 0.352% under second pinch roll, nearly reached the critical strain, so the cracks may appear.

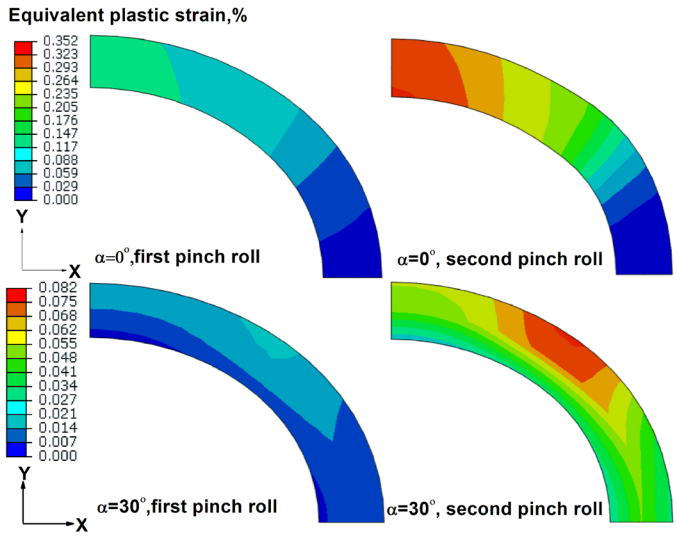

Fig. 5. The equivalent plastic strain in the brittle temperature range with soft reduction

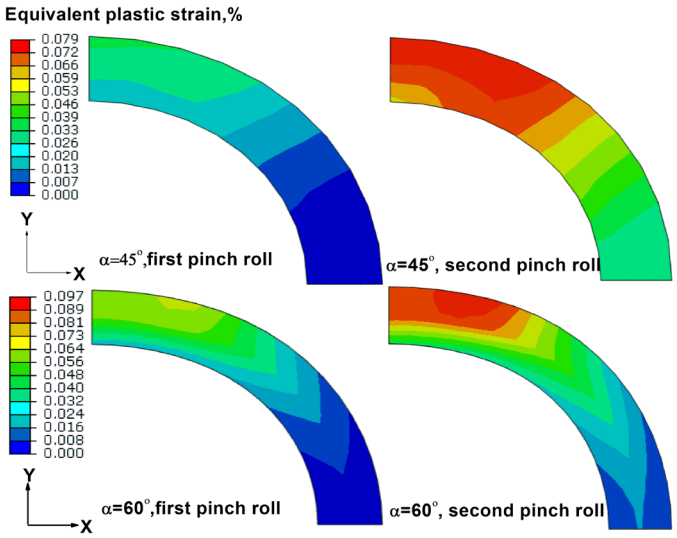

Fig. 6. The equivalent plastic strain in the brittle temperature range with soft reduction

Due to the fact that the risk of the occurrence of cracks clearly decreases with chamfer billet. By using the chamfer billet, the high reduction could be taken and avoided especially at the beginning of the reduction process. According to the simulated results, the optimized soft reduction process can be developed to avoid the formation of internal cracks by the change of α. The variation tendency of equivalent plastic strain shows reasonable similarity to the maximum of maximal principal stress in the brittle temperature range during soft reduction. Therefore, the compressive stress and stress region of billet was remarkably improved by increasing the incensement of α in comparison with that by the conventional soft reduction. This is because the geometry of the chamfer billet compresses the mushy zone effectively during deformation as shown in Fig. 6. This study reveals that the thickness reduction of 2 mm minimizes the creation of internal cracks when the chamfer billet is used in the soft reduction process.

It can be seen from that the distribution of maximal principal stresses is the largest when the position is under deformation, the distribution of maximal principal stresses have the same tendency by the first pair pinch rolls reduction and the second. Due to this reason, only the maximal principal stresses under the rolls reduction are studied in following discussions. The maximal principal stresses under the second pair pinch rolls reduction are small larger than the first pair pinch rolls reduction, as shown in Fig. 7 and Fig. 8. When the angle of billet is 45°, the interval values between the first and second pair pinch rolls reduction is smaller than the others. Fig. 9 and Fig. 10 illustrate the configuration of the maximal principal stresses in the soft reduction process, viewed from the side, which shows the conventional configuration of the rectangular billet and chamfer billet, which is casting for 45s and reducing by one pair pinch roll in a specific zone. And the amount of reduction is 2 mm. In order to obtain the degree of internal crack in the brittle temperature range, the maximal principal stresses at different reduction positions before (Fig. 9(a) and Fig. 10(a)), under (Fig. 9(b) and Fig. 10(b)) and after (Fig. 9(c) and Fig. 10(c)) reduction have been determined.

The evolution of internal stress of rectangular and chamfer billet at the cross section under reduction process is depicted in Fig. 9(b) and Fig. 10(b) respectively. When the billet entered into the roll zone, there was a certain stress gradient between the surface and core parts of the billet due to non-uniform deformation. This resulted in the phenomenon where the stress distribution in the cross section was inconsistent along the height direction. At the contact surface between the pinch roll and billet, the surface part was subjected to compressive stress, while the core part was subjected to tensile stress. In cross section of the rectangular billet along the width direction, the maximal compressive stress exceeded the compressive stress from the center to the edges gradually, then the compressive stress decreased and it even turned into tensile stress at the corner side. While the maximal compressive stress of chamfer billet is existed at the middle part, this led to a greater contraction at the middle part compared with the edges. It can be seen that the distribution of the stress was non-uniform in the thickness and width directions. This maximum tensile stress in the brittle temperature range is

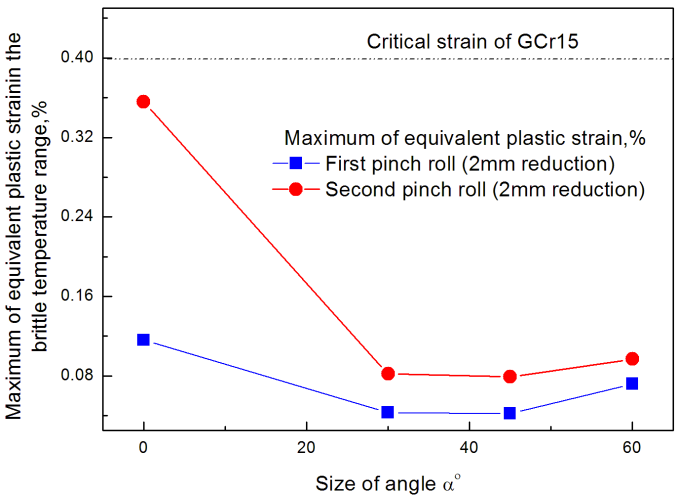

Fig. 7. Maximum of equivalent plastic strain in the brittle temperature range during soft reduction

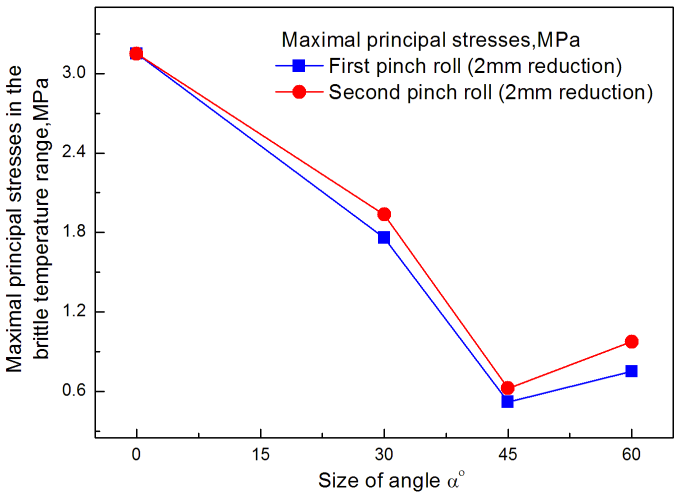

Fig. 8. Maximal principal stresses in the brittle temperature range during soft reduction

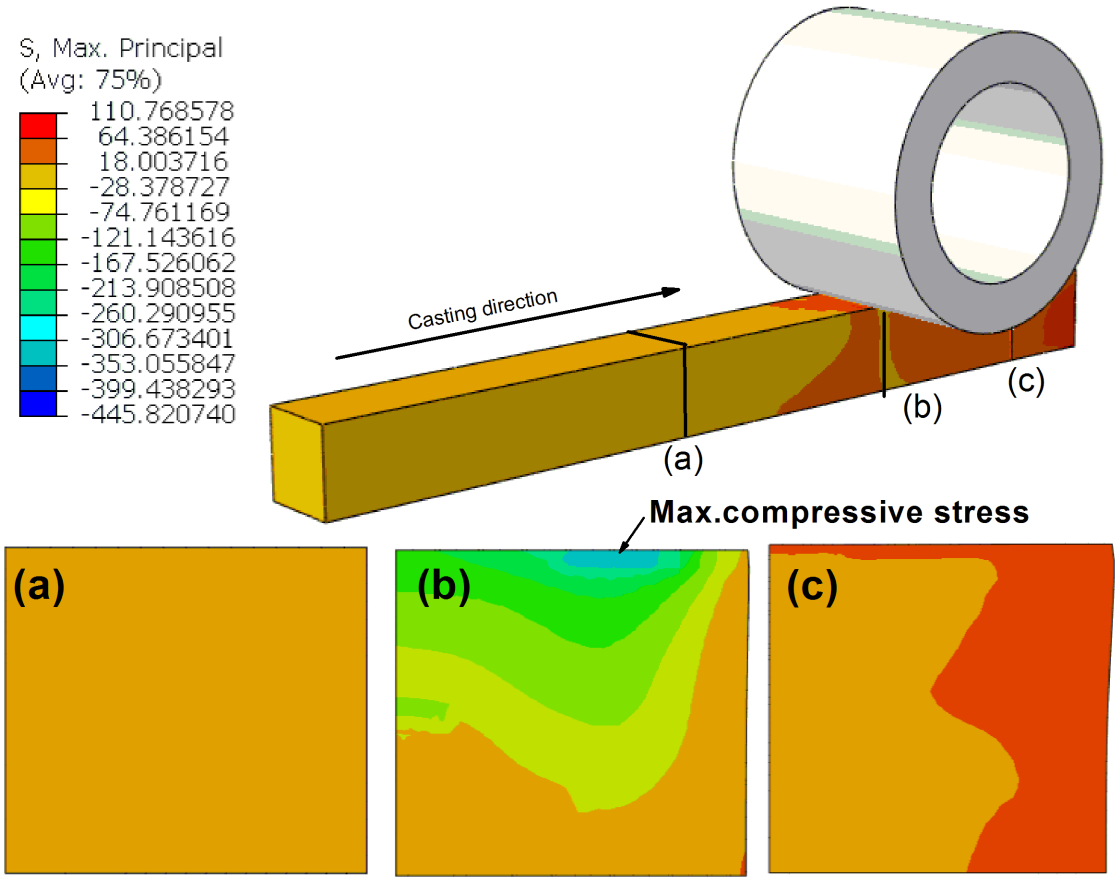

Fig. 9. Maximal principal stresses evolution of rectangular billet at different position along the longitudinal direction (in unit of MPa)

more sensitive to the risk of internal crack. The stress distribution of rectangular and chamfer billet at the cross section after deformation is shown in Fig. 9(c) and Fig. 10(c), respectively. It was observed that the tensile stress of rectangular billet was more prominent than that of the chamfer billet at the brittle temperature range. This was directly related to the relatively formation of internal crack.

In order to reduce the risk of internal cracks in the brittle temperature range, increasing chamfer angle is more effective way to get the higher reduction efficiency. The same reduction effect with larger reduction and lesser internal crack risk can be obtained by adjusting the chamfer angle of the billet. It is notable that chamfer billet after soft reduction, the risk of internal cracking and centre porosity of the billet is improved. The reduction force decreases obviously and the billets casting process with chamfer geometries is suitable for the heavy reduction technology due to the energy required in deforming the billets decreases significantly.

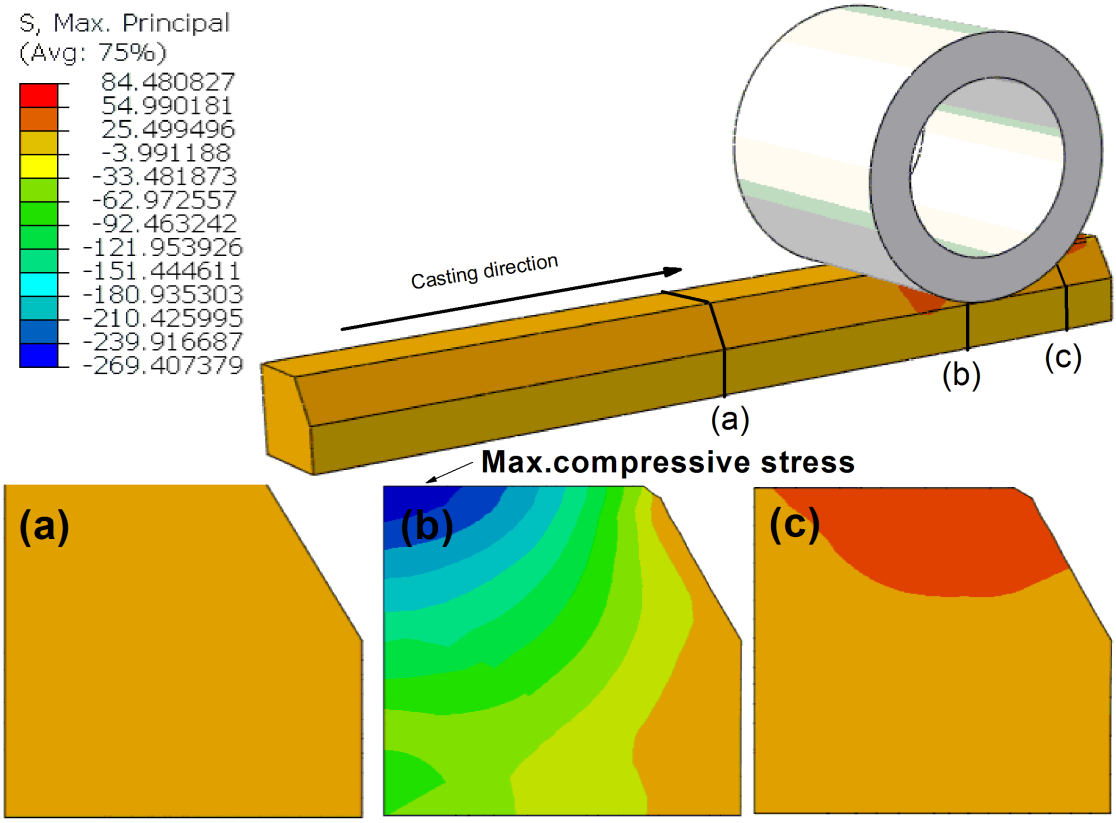

Fig. 10. Maximal principal stresses evolution of chamfer billet at different position along the longitudinal direction (in unit of MPa)

4. Conclusion

(1) The brittle temperature range of GCr15 bearing steel is between 1305°C and 1366°C, which is calculated by the solidification phase transformation model.

(2) The compressive stress area of as-cast billet was remarkably enlarged by increasing the incensement of α in comparison with that by the conventional soft reduction. The chamfer configuration of as-cast billet compresses the mushy zone effectively during soft reduction. The maximal principal stress and the tensile stress in as-cast billet decrease with the increase of chamfer angle.

(3) The maximum of equivalent plastic strain of chamfer billet is lower than that of rectangular billet. According to the simulated results, the optimized chamfer configuration of as-cast billet can be developed to decrease the risk of internal cracking by the adjustment of chamfer angle.

(4) The maximal principal stresses under the second pair pinch rolls are a little larger than the first pair pinch rolls reduction. When the angle of billet is 45°, the interval values between the first and second pair pinch rolls reduction is smaller than the others.

Acknowledgement

The present work is financially supported by The National Key Research and Development Program of China No. 2017YFB1103700.

REFERENCES

[1] H.K.D.H. Bhadeshia, Steels for bearings, Progress in Materials Science **57**, 268-435 (2012).

[2] S. Luo, M.Y. Zhu, C. Ji, Theoretical model for determining optimum soft reduction zone of continuous casting steel, Ironmaking and Steelmaking **41**, 233-240 (2014).

[3] J. Zhao, L. Liu, W. Wang, H. Lu, Effects of heavy reduction technology on internal quality of continuous casting bloom, Ironmaking and Steelmaking **46**, 227-234 (2017).

[4] K.H. Kim, T. Yeo, K.H. Oh, D.N. Lee, Effect of carbon and sulfur in continuously cast strand on longitudinal surface cracks, ISIJ International **36**, 284-290 (1996).

[5] A. Cwudziński, Numerical and physical simulation of liquid steel behaviour in one strand tundish with subflux turbulence controller, Archives of Metallurgy and Materials **60**, 3, 1581-1586 (2015).

[6] A. Cwudziński, Numerical and physical modeling of liquid steel behaviour in one strand tundish with gas permeable barrier, Archives of Metallurgy and Materials **63**, 2, 589-596 (2018).

[7] T. Merder, Numerical analysis of the structure of liquid flow in the tundish with physical model verifocation, Archives of Metallurgy and Materials **63**, 4, 1895-1901 (2018).

[8] T. Merder, Modelling the influence of changing constructive parameters of multi-strand tundish on steel flow and heat transfer, Ironmaking and Steelmaking **40**, 10, 1743-2812 (2016).

[9] T. Merder, Influence of design parameters of tundish and technological parameters of steel continuous casting on the hydrodynamics of the liquid steel flow, Metalurgija **53**, 4, 443-446 (2014).

[10] X.B. Li, H. Ding, Z.Y. Tang, Formation of internal cracks during soft reduction in rectangular bloom continuous casting, International Journal of Minerals, Metallurgy and Materials **19**, 1, 21-29 (2012).

[11] N. Zong, H. Zhang, Y. Liu, Z. Lu, Analysis on morphology and stress concentration in continuous casting bloom to learn the formation and propagation of internal cracks induced by soft reduction technology, Ironmaking and Steelmaking **46**, 9, 872-885 (2019).

[12] N. Zong, Y. Liu, H. Zhang, X. Yang, Application of a chamfered slab technology to reduce straight edge seam defects of non-oriented silicon electrical steel generated during flexible thin slab casting process, Metallurgical Research & Technology **114**, 311-319 (2017).

[13] N. Zong, Y. Liu, H. Zhang, Application of chamfered narrow face mold technology to reduce longitudinal surface crack defects of hyperperitectic steel generated during flexible thin slab casting process, Metallurgical Research & Technology **114**, 413-421(2017).

[14] T.W. Clyne, M. Wolf, W. Kurz, The effect of melt composition on solidification cracking of steel, with particular reference to continuous casting, Metallurgical and Materials Transactions B **13**, 259-266(1982).

[15] Y. Ueshima, S. Mizoguchi, T. Matsumiya, Analysis of solute distribution in dendrites of carbon steel with δ/γ transformation during solidification, Metallurgical and materials transactions B **17**, 845-859 (1986).

[16] K. Kim, H.N. Han, Y. Lee, Proc. Conf. Melt cpinning, ctrip casting and slab casting, TMS, Warrendale, PA, Anaheim, 87, (1996).

[17] N. Zong, H. Zhang, Y. Liu, Z. Lu, Analysis of the off-corner subsurface cracks of continuous casting blooms under the influence of soft reduction and controllable approaches by a chamfer technology, Metallurgical Research & Technology **116**, 310-322 (2019).

[18] N. Zong, Y. Liu, S. Ma, W. Sun, T. Jing, H. Zhang, A review of chamfer technology in continuous casting process, Metallurgical Research & Technology **117**, 204-219 (2020).

[19] Y. Fei, H. Lin, M. Huajie, H. Xinghui, Constitutive modeling for flow behavior of GCr15 steel under hot compression experiments, Materials & Design **43**, 393-401 (2013).

[20] Y. Hou, T. He, S. Chen, H. Ji, R. Wu, Microstructure evolution and unified constitutive equations for the elevated temperature deformation of SAE 52100 bearing steel, Journal of Manufacturing Processes **44**, 113-124 (2019).

[21] P.F. Kozlowski, B.G. Thomas, J.A. Azzi, H. Wang, Simple constitutive equations for steel at high temperature, Metallurgical and materials transactions A **23**, 903-918(1992).

[22] Y.M. Won, B.G. Thomas, Simple model of microsegregation during solidification of steels, Metallurgical and materials transactions A **32**, 1755-1767(001).

[23] A. Yamanaka, K. Nakajima, K. Okamura, Critical strain for internal crack formation in continuous casting, Ironmaking and Steelmaking **22**, 508-512 (1995).

[24] Hiebler, J. Zirngast, C. Bernhard, M.M. Wolf, Inner crack formation in continuous casting: stress or strain criterion? In: Steelmaking Conf. Proc. **77**, 405-416 (1994).